Proceedings of GPPS Forum 18
Global Power and Propulsion Society
Montreal, 7th-9th May 2018
www.gpps.global

GPPS-2018-0072

Sensitivity analysis of eigenmode variations on the flutter stability of a highly loaded transonic fan

Senad Iseni
Chair of Thermal Turbomachines and Aeroengines
senad.iseni@rub.de
Bochum, Germany

Derek Micallef
Chair of Thermal Turbomachines and Aeroengines
derek.micallef@rub.de
Bochum, Germany

Francesca di Mare
Chair of Thermal Turbomachines and Aeroengines
francesca.dimare@rub.de
Bochum, Germany

ABSTRACT

This paper focusses on the flutter analysis of a scaled high-speed fan. The fan performance prediction is validated against rig data using Reynolds-Averaged Navier-Stokes (RANS) CFD simulations. All flutter stability calculations are based on the energy exchange approach which is used to predict the whole flutter map for the first bending mode, for which flutter occurs. In order to save computational time, the requirements of the influence coefficient formulation (ICM) were verified by an amplitude and blade passage number study. Afterwards, the ICM was compared against the travelling wave mode method (TWM). Only one unsteady CFD calculation has to be performed to reconstruct the whole stability curve for a specific eigenmode and operating point, which is a major benefit of the ICM. Key parameters of flutter stability such as shock-related effects and tip gap flows are identified and investigated at off design and part speed conditions. Flutter instabilities occur downstream of the suction side because of the shock structure which leads to a high pressure gradient in that region. The presence of the shock induces separated or nearly separated flows with greater pressure amplitudes and phase changes. Additionally, an eigenfrequency and mode shape variation is carried out for a blade-only model (no blade roots) to determine their influence on the fan flutter stability. For this purpose, the impact of twist/plunge ratio for the first flap mode shape is investigated. In addition to that, the first mode shape of a blade model is considered including nonlinear contacts at the blade root within a static structural analysis and compared against the blade only model. The results show that suppression of flutter onset can be achieved for specific constellations of structural parameters.

INTRODUCTION

Modern aero-engines have to meet high requirements regarding engine safety, economic and environmental aspects. Technical challenges for modern aero engines are the development of designs which enables a reduced noise emission and high aerodynamic efficiency. Aeroelastic stability of fans is especially influenced by flow driven mechanisms, which limits the safety operating range of aero-engines [1,2]. Restrictions in the fan operating conditions results from an aerodynamically self-excited vibration at a resonance state of the fan, where fluid energy will be transferred into the vibrating blade and can yield to blade failure. Key parameters, that influence flutter stability are given by e.g. Srinivasan [3]. The so-called acoustic flutter, which may occur due intake pressure wave reflections created by the blade vibration [4-6] is not assessed in this study. In addition to the above mentioned mechanisms, the fan stability is also affected by structural characteristics, like the eigenfrequency and mode shape of the fan blade. The more classic application of the reduced frequency criterium is exclusively geometrical restricted at constant span locations defined by the chord length. In combination with simple reduced frequency Vahdati and Cumpsty [7] use the amount of plunge-to-twist ratios of mode shapes as a design criterion.

Nevertheless, non-linear CFD analyses are required for a detailed flow description to capture high three-dimensional flow excitations to predict flow driven flutter instabilities and ensure a flutter free fan design. The classic approach based on the energy-exchange method is used to predict single-mode flutter boundary with aid of the Influence Coefficient Method (ICM). Focus of this paper is a comprehensive flutter analysis of modified eigenmodes due to twist/plunge ratio and eigenfrequency variations. Aerodynamic and geometric key parameters of the highly loaded transonic fan, which contribute to flutter risk or flutter onset will be also discussed.

ANECOM FAN ROTOR R1

The UFFA-Fan Stage of the AneCom Aerotest GmbH was adopted as model for the purpose of this numerical study. A 1/3-scale model for the fan, also called ACAT

(AneCom AeroTest) Rotor R1, was considered. Design parameters as well as main characteristics are listeted in Table 1. The UFFA is a modular fan rig, which is designed to satisfy the need for advanced investigations of fan noise. By using a turbulence control screen (TCS), the inflow control device enables for all speeds a comparison of measurements on static test beds and flight tests.

Table 1: AneCom ACAT Rotor 1 from UFFA

Rotor diameter [mm]	869
Hub-to-tip ratio [-]	0.3
Fan blade count [-]	20
Relativ tip Ma (DP) [-]	1.2
Fan pressure ratio (DP) [-]	1.5
Max. massflow [kg/s]	118
Max. rig speed [rpm]	10,000

Fan performance steady data are made available by AneCom and are used for validation purposes. Measurements in the rotating frame of reference were taken by using strain gauges mounted on the rotor. The strain gauge signals were recorded at a sampling rate of 48 kHZ and used to validate the URANS flutter stability simulations. A more detailed description of the test facility is given by Köhler [8] and Mueller et al. [9]. This Fan-Stage was also used in a previous multidisciplinary numerical study to investigate the influence of outer casing modifications in an aero-acoustic optimization loop [10].

FLUTTER STABILITY ANALYSIS MODEL

Aerodynamic Flow Model

RANS simulations have been performed using the parallelized, multiblock, finite-volume compressible flow solver TBLOCK, which was further extended for flutter analyses by Micallef et al. [11,12]. The Spalart-Allmaras turbulence model has been adopted. A more generalized version of the Phase-Shifted-Boundary-Condition (PSBC) approach was implemented, which allows flutter stability predictions with respect to multiple flow disturbances such as a total pressure inlet distortion pattern [12,13]. First successful validation results for 3D viscous flutter analyses in turbine cascades for subsonic and transonic follow regimes are shown in [11] and in supersonic flow by Witteck et al. [14]. The Fan-model was used in a previous numerical study to investigate the influence of outer casing modifications on the flutter boundaries [11].

A description of the block-structured CFD grid size is given in Table A in the appendix. A one-to-one connected grid topology is used within the tip gap (butterfly-topology) to avoid the need of interpolation between neighboring blocks. Blade and end-wall surfaces were treated as adiabatic boundaries and a logarithmic wall function is used to calculate the wall shear stresses. The inlet boundary condition is defined by constant pitch-wise averaged stagnation flow values (total pressure/ temperature and flow angles) resulting from measurements in the test facility. At the outlet of the computational domain non-reflecting boundary conditions and a radial equilibrium pressure distribution is used. The static pressure is specified at the hub, which has led especially near stall to robust flutter computations. It is not within the scope of this study to assess induced acoustic flutter based on blade vibrations. Furthermore, it was shown during the measurements, that the TCS does not excite additional acoustic modes.

Structural Models

Due to high rotational speeds and steady pressure loads, the manufactured blade geometry results in blade untwist. For that reason, deformations are iteratively computed under steady loads at aerodynamic stability limits near stall/surge. Apart from steady pressure loads, centrifugal loads through the fan rotation have to be considered for the manufactured geometry as described e.g. in [13]. The influence of steady deformations on the numerical flutter prediction for highly loaded and flexible fan blades was investigated in detail by Schuff [15] at off-design conditions. It was pointed out that especially torsional deflections in regions of near stalled conditions have a significant influence on the flutter boundary prediction. It will be shown, that the twist/plunge ratio α depends also on the rotational speed. Static finite element analysis (FEM) were performed up to the design speed line considering iterative stiffness matrix updates due to geometric nonlinear deformations. Pre-stressed modal analyses are carried out for the first eigenmode including the blade fir-tree root and disk conjunction. The high mechanical loads at the contact areas of the fir-tree joint are investigated for different shaft speeds and friction coefficients using the commercial FEM solver ANSYS. The nonlinear contact problem is solved using the Augmented-Lagrange-method. The maximal equivalent von Mises stresses at the blade root are within the safety margins corresponding to the yield strength. The maximal static deformation for the fan is 2.34% (trailing edge at tip moving towards the suction side) with respect to the blade tip chord length C. The first eigenmode was detailed investigated, due to the fact that the bending mode shows lowest flutter stability.

Numerical FSI-Method

The most common numerical methods for flutter analyses are based on the energy exchange approach. No changes in structural properties are assumed due to unsteady aerodynamic blade loading. To investigate the flutter risk behaviour a one-way fluid structure-interaction (FSI) is applied. The aerodynamic work W_{aero}

$$W_{aero} = \int_t^{t+T} \int_A -\left(\dot{\mathbf{x}}\mathbf{n}p\right) dA\, dt \qquad (1)$$

done by an unsteady flow field is calculated on the blade during one period of blade vibration T. The energy transfer takes place on the blade surface A. Aerodynamic force

contribution results from a projected pressure field in modal direction, defined by the mode shape. The flutter stability is then expressed by the logarithmic decrement Λ,

$$\Lambda = \frac{-W_{aero}}{2E_{kin,max}} \qquad (2)$$

where a negative Λ value indicates flutter risk and results in energy being transferred from surrounding fluid to the blade structure and might lead to an amplified amplitude blade vibration. In order to predict the flutter stability two different formulations, the ICM formulation and TWM-Method, are taken into account

AERODYNAMIC PERFORMANCE AND FLUTTER STABILITY VALIDATION

The steady mean flow for each fan speed line is obtained by increasing the static back pressure starting from an operating point near choke line. The calculated aerodynamic performance map for the baseline design is shown in Figure 1. The fan pressure ratio and mass flow are referred to peak

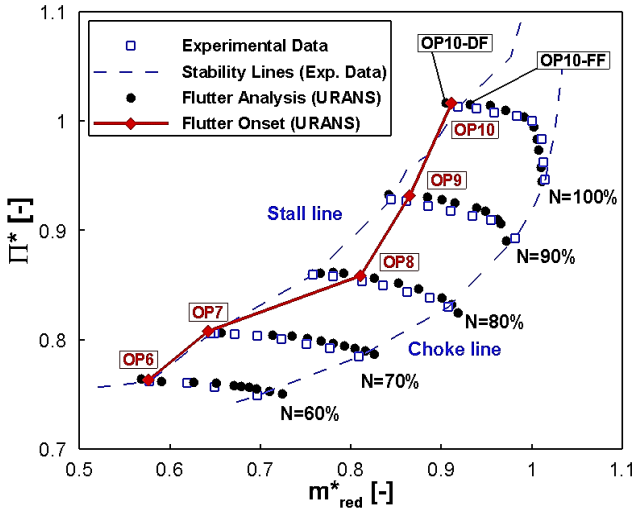

Figure 1: Fan performance map and flutter boundary

efficiency at 100% speed. In comparison with measured speed lines with respect to fan pressure ratio and reduced mass flow the steady mean flow is well captured and shows good agreement with the measurements. The operating range at part speed (80% and 90%) is restricted by the fan flutter line and not by the stall/surge boundary. The calculated flutter onset operating points OP6-OP10 have regarding their mass flows in comparison with the measurements a maximum difference of 1.7% at OP10. The maximum pressure ratio difference is determined at OP9 at 90% design speed with an amount of 1%. The appearance of shocks has shown a significant impact and contributes to reducing the fan flutter stability. Vahdati et al. [1] as well as Srivastava et al. [16,17] observed and reported a strong shock impact on flutter stability within the operating range especially at part speed. Furthermore, the fan configurations investigated here is showing an influence of tip leakage flow on flutter stability. The first fan mode shape undergoes not only a pure plunge motion, but has also a high twist component, which will be discussed later. The maximal vibration amplitude is observed at the fan tip leading edge, which will introduce a high level of pressure disturbances.

Blade Amplitude Variation and Passage Number Study

The underlying assumptions of the energy approach (see previous sections) have been verified by carrying out a blade vibration amplitude analysis. On this account a blade vibration amplitude study was carried out in the TWM formulation at the operating point OP10. The assumption of

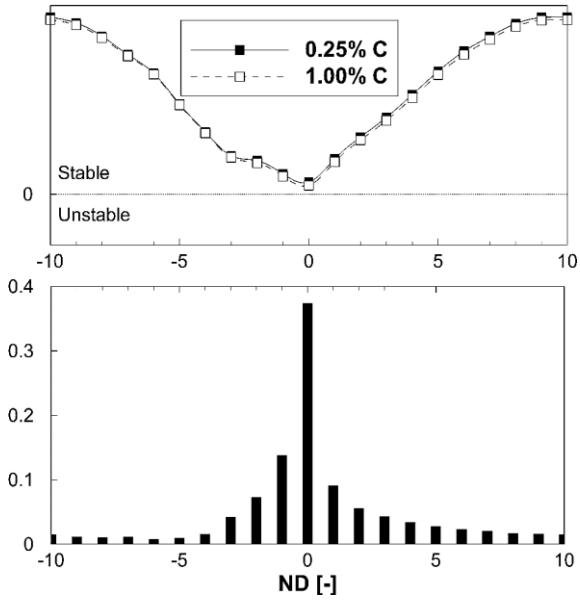

Figure 2: Amplitude study at OP10

linearity of the fluid-structure coupling was verified near stall/surge at design speed. A maximal vibration amplitude of 0.25% of the blade tip blade chord length (0.25% C) as well as a four times higher (1.00% C) amplitude was forced for the blade motion, as shown in Figure 2. The implemented moving mesh algorithm and the interpolation routine for mode shapes are used to update the three-dimensional CFD mesh. The considered operating point is flutter as shown at the top of Figure 2. It was observed that the aerodynamic work W_{aero} is also directly proportional to the square of the maximum vibration amplitude at the corresponding ND. Both calculated flutter stability curves show a good agreement regarding the Λ-values over the whole ND range and global minimum (ND 0) as shown in Figure 2 at the top. In addition to that, the percentage stability difference for both prescribed vibration amplitudes is shown at the bottom of Figure 2. The highest flutter stability difference exists for the global minimum at ND 0 with an amount less than 0.4%. The deviations are decreasing for higher ND's. Nevertheless, the same flutter stability curve was sufficient achieved independent of the prescribed vibration amplitude and agree well to each other to be within the scope of the energy

method. This justify the linear system behavior assumption in an uncoupled flutter calculation.

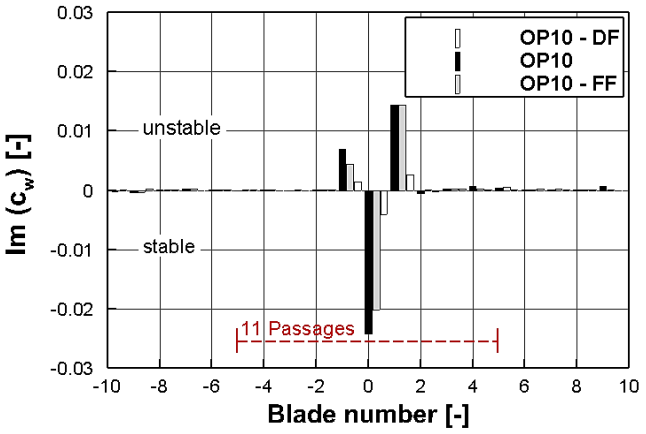

Figure 3: Influence coefficients at design speed

To save computational time a determination of the correct blade passage number for IC-Method is purposed to capture almost the same results as the TWM-Method. For this purpose, an inverse strategy was started to capture the influence of neighboring blades during the blade vibration. Therefore, influence coefficients based on the TWM flutter calculations are determined for the baseline at three operating points. The imaginary part $\mathrm{Im}[\hat{c}_w]$ of the influence coefficients are shown as bars in Figure 3 for a flutter free, flutter (OP10-FF) onset (OP10)and a deep flutter (OP10-DF)

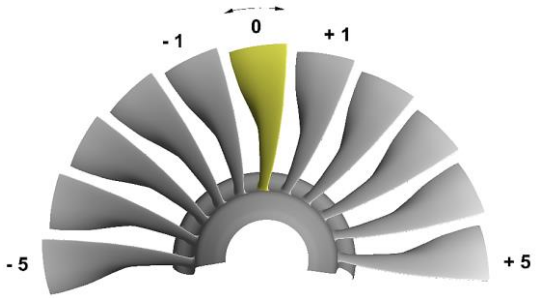

Figure 4: ICM-Model (11 Passages) for mode 1

condition at design speed. The vibrating fan blade 0 shows at all operating points a stable contribution on the overall flutter stability and determines primarily the stability behavior. The unstable contributions of direct neighboring blades (± 1) are much higher compared to the other blades. The influence of neighboring blades decreases with growing distance to the reference blade. Moreover, it can be noticed that an increased number of influence coefficients are required at unstable flow conditions to predict the flutter stability as in TWM. To accurately predict the global flutter stability minimum and reduce the computational effort a blade passage number of 11 blades was selected to conduct further numerical studies. The multi-passage model in Figure 4 is used for the ICM computation domain, where only the reference blade 0 oscillates. Using PSBC based on the Shape Correction Method (SCM) a two blade passage model can be used for the TWM. In contrast to that, a multi blade passage is required for the ICM using periodic boundary conditions (PBC).

Flutter Onset

In addition to that the operating point OP8 at 80% design speed is considered for validation purposes against available experimental data. A 1.3% lower mass flow and a 0.5% higher predicted pressure ratio is determined compared to the measurements, whereby the aerodynamic blade loading at OP8 is well captured. A total number of 8 blades are instrumented with two strain gauges, which are located in a

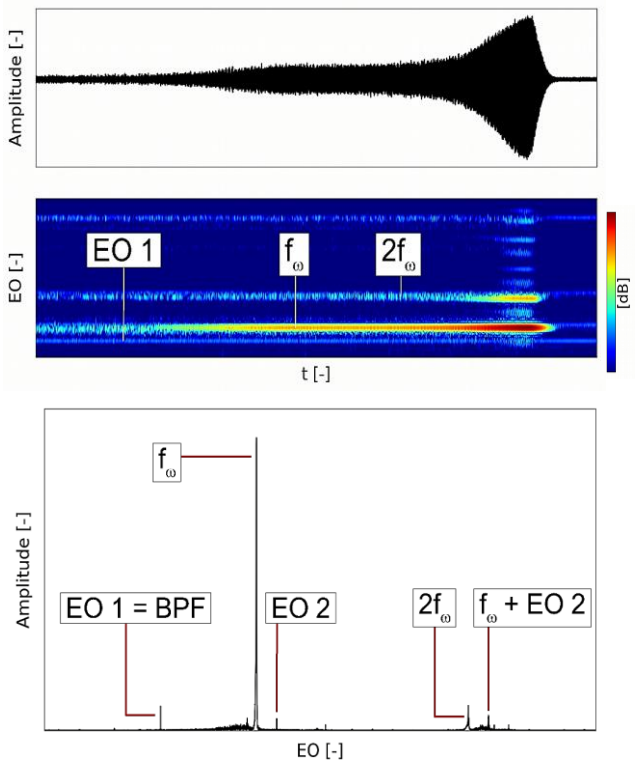

Figure 5: Top: Time history; middle: spectrogram; bottom: frequency spectra at OP8

parallel grid arrangement at the leading and trailing edge. These gauges are applied on the pressure surface without any contact to the fillet radius.

Figure 5 (top) shows the time history of the measured fan strain gauge signal for blade 1. The frequency spectra were computed from 12,000 samples using a Hamming window with an overlap of 50%. The flutter onset is clearly visible on the spectrogram (Figure 5 middle) due to the fact that the high amplitude amplifications will reach the resonant point. The eigenfrequency lies between EO 1(BPF 1) and EO2 (BPF 2) at 80% design speed, which is also visible in Figure 5 (bottom). All other harmonics or their linear combinations, showing significant lower amplitudes, are excluded from the eigenfrequency analysis. The flutter stability computations are based on the blade eigenfrequency and BPF, which finds

corroboration in the measurements. The chosen flutter stability analysis method is therefore applicable to resolve the unsteady flow field with the dominant harmonics using the previous mentioned SCM method, which is based on the prescribed frequencies as shown in [11]. The maximum deviation of the prestressed modal analysis computations (blade only model) based on the measured flutter frequency is +3%. For the nonlinear simulations including root-disk a 3% lower deviation compared to the measurements was observed These uncertainties are within the 10% safety limit to EO 2. At 80% part speed a backward travelling wave of ND -3 was identified, which results in a flutter condition.

MODESHAPE AND EIGENFREQUENCY FLUTTER ANALYSIS

In the following sections the effect of twist/plunge ratio and blade eigenfrequency variation on the flutter stability boundary will be discussed. Special attention is also given to the operating point OP8 at 80% part speed with the lowest flutter margin near stall limit.

Twist/Plung Ratio and Eigenfrequency Variation

To modify the twist/plunge ratio the medial axis transformation method was used to determine leading and trailing edges. This efficient approach is mainly based on profile boundary (free-form curves) tracing and decompositions using general geometric algorithms [18].
A projection of modal displacements in chord direction was

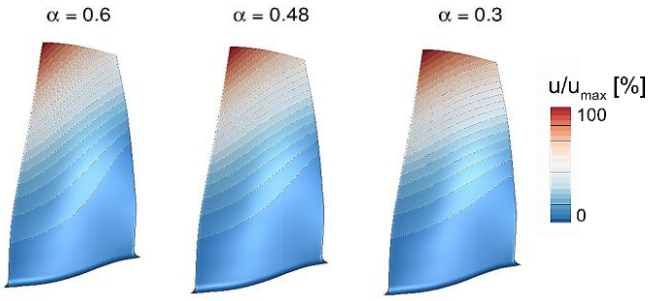

Figure 6: Modified 1F mode shapes

performed to determine the pure plunge component motion as described in [7]. Twist components were determined by subtracting absolute displacements from the pure plunge components. The twist/plunge ratio can be described as follows,

$$\alpha = (x_{LE} - x_{TE})/(0.5(x_{LE} + x_{TE})) \qquad (3)$$

where x_{LE} and x_{TE} are the magnitudes of LE and TE edge displacements, respectively. The contour plot in Figure 6 represents absolute displacements for the baseline (center) as well as two scaled mode shapes. The baseline mode shape at the blade tip has a maximal ratio of α=0.48 at 80% part speed. The twist components were modified to investigate the effect of mode shapes on the flutter stability. A reduction of α leads to an increased modal displacement contribution near the trailing edge. The radial distribution of the modal

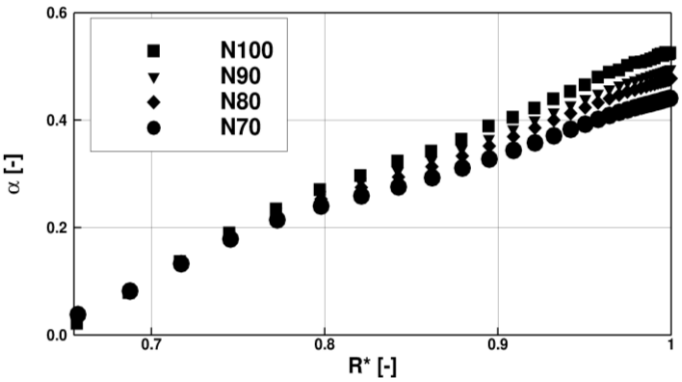

Figure 7: Twist/plunge ratio vs. blade span as a function of the fan shaft speed

displacement components for α=0.48 are given in the appendix in Figure B1. The trailing edge twist over the radius shows a nearly constant trend compared to the other displacement components and shows in the opposite direction. This fact leads to a lower absolute displacement at the trailing edge. Figure 7 shows the radial distribution of α as a function of the fan shaft speed. With increasing shaft speeds an increase of α is observed with a greater effect at the blade tip. A higher value for α results in a higher twist amplitude, especially at leading edge.

The eigenfrequency variation f^* [2] is based on f_ω as well as the maximal modified frequency f_{max}:

$$f^* = (f_i - f_\omega)/(f_\omega - f_{max}) \qquad (4)$$

A flutter stability analysis is performed for the normalized frequencies in a range between f^*= - 0.5 and f^*= 1.0.

Throat Area Variation

Accompanied by the motion of the blades, the geometric channel region between two blades is either expanded or contracted. The flow channel area also depends strongly on the IBPA between blades. A twist/plunge ratio modification results also to a flow passage area variation during a blade vibration oscillation. For this purpose, the channel kinematic considered and used to assess the aerodynamic as well as flutter stability. The channel kinematic as well the used notation in this paper are shown in the appendix in Figure B2. Two vibrating blades with a specified eigenfrequency f_ω are considered. The pure geometric channel s(t) (here also defined as passage medial axis) is described using the medial axis formulation as shown in Figure B2. A non-zero ND at time t_0=0 and $t > t_0$ will be assumed during blade vibration. The throat area $A(s_0, t)$ is time and location-dependent. The effective flow passage is generally reduced due to the boundary layer thickness [20], however this effect will not be considered here. Starting from the throat area $A(s_0, t)$ the passage area, at a constant radius, is growing continuously and reaches a maximum downstream at $A(s_n, t)$. In contrast the throat area, greater amplitude variations $\Delta A(s_0, t)$ and lower amplitudes can be observed at the remaining location

$A(s_i, t)$. A BTW compared to a FTW keeping the IBPA constant results here only in a phase difference for the throat area. Increasing the IBPA results in increased geometric passage variation $\Delta A(s_i, t)$.

Flutter Stability Results

It was observed that mode shape modifications can lead to a shift of the global flutter minimum Λ with respect to the ND of the baseline design. Figure 9 shows the flutter stability as a function of f^* for three ND's at 80% part speed.

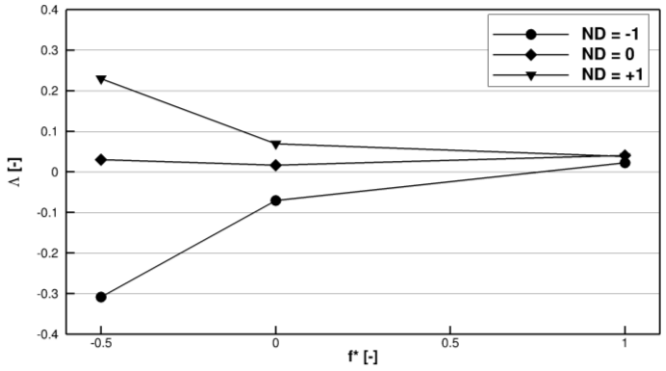

Figure 9: Flutter stability vs. f^* at OP8

In this case only the frequency was changed, keeping the twist/plunge ratio of the baseline design constant. For the BTW at ND -1 a growing blade frequency f_ω leads to an increased stability. The opposite trend is observed for the FTW ND +1. The impact of f_ω on ND 0 is negligible. It can be concluded that a frequency variation f_ω for non-zero ND's leads to an significant change in fan flutter stability, especially at $f^* < 0$. Nevertheless, it is obvious that the global minimum at 80% design speed exists for a BTW of ND -3.

Figure 10 (top) shows the results of the flutter stability analysis as a function of the fan shaft speeds and blade frequencies at the flutter boundary (OP7 - OP10). The twist/plunge ratio is kept constant ($\alpha = 0.48$). An Increased flutter margin was achieved for $f^* > 0$, except at 80% part speed. No stability improvements are apparent due to frequency variations at 80% part speed, however, the flutter margin grows especially at 70% design speed. After this first eigenfrequency study, the fan baseline eigenfrequency is kept constant ($f^* = 0$) and only a twist/plunge ratio variation was applied. Only the highest ratio ($\alpha = 0.6$) leads to a stability reduction for all considered speed lines at the flutter boundary, as shown in Figure 10 (bottom). Despite that, analysing the trend due to α- modification is a promising approach because this leads to less flutter stability variations Δ Λ than the previously discussed blade eigenfrequency modification.

A combination of both design parameters (f^* and α) will be also investigated at OP8 in the following sections. To achieve a high flutter stability variation Δ Λ, flutter stability analysis were performed for each combination to identify an

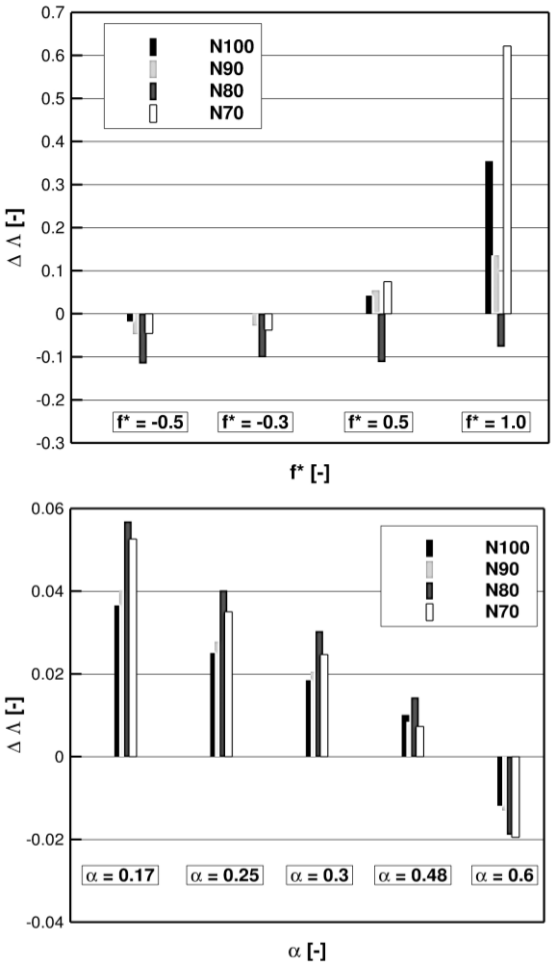

Figure 10: Top: Flutter stability variation vs. f^*; bottom: flutter stability variation vs.

optimal structural modification. By considering of $f^* = 0$ a flutter-free design could not be achieved only by reducing of α. However, by a combination with the other f^*values ($f^* \neq 0$) an increased stability could be reached. Even so, a high

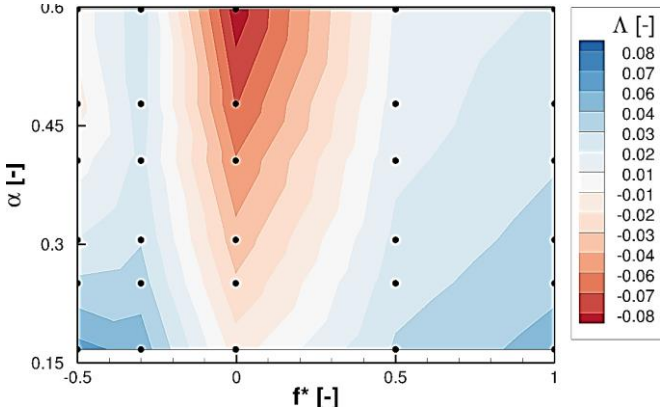

Figure 11: Flutter stability contour at OP8

flutter risk for $f^* = -0.5$ and α=0.48 (baseline twist/plunge ratio) was identified. As shown in Figure 11, both extrema of f^* (-0.5 or 1.0) in combination with low α ratios seem to

ensure a high flutter stability. Flow-driven mechanisms also play a role in affecting flutter stability near stability limit. A relative tip Mach number close to 1 was achieved at this operating point at 80% part speed. It was observed that the shock position moved towards the blade leading edge with lower mass flows along the speed line. The shock is located on the suction side near the leading edge and occurs already

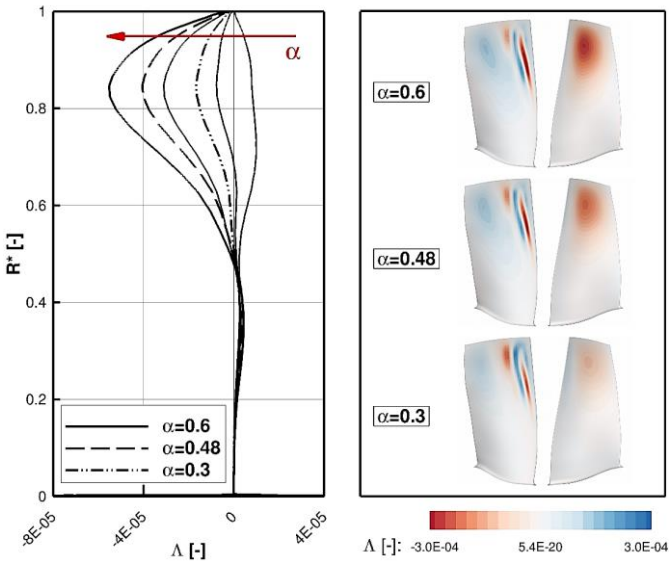

Figure 12: Radial (left) and local flutter stability distribution (right) at OP8

at 30% span. This results to an instability region on the suction side starting from 50% span to tip, which is shown in Figure 12.

The radial and local stability distribution for the baseline frequency $f^*=0$ on the blade surfaces due to the effect of twist/plunge ratio modifications is also shown for $\alpha=0.3$, $\alpha=0.48$ and $\alpha=0.6$ in Figure 12. Flutter instabilities occur downstream of the shock due to a high pressure gradient, which induces a separated or nearly separated flows with increased pressure amplitudes and phase changes.

An unstable Λ-distribution also exists on the upper half on the pressure side but it is rather influenced by the unsteady pressure field from the tip clearance flow. Moreover, the shock position determines the stabilizing/destabilizing transition areas. Thus, it can be concluded that a local transonic region mainly drives the flutter instability. A lower α-value leads to an increased stability on both blade surfaces, especially on the upper half side of the pressure surface. On the other hand, a weaker reduction on the suction side downstream of the shock is visible. For this reason, the Mach number variation as well as the corresponding shock oscillation amplitude on the suction side were investigated as shown in Figure 13 at 80% blade span. The Mach number fluctuation at this operating point conditions seems to behave in a non-linear, dynamic way, to the shock oscillation with increased α. The corresponding percentage throat area variation for $\alpha=0.3$, $\alpha=0.48$ and $\alpha=0.6$ is given in Figure 14.

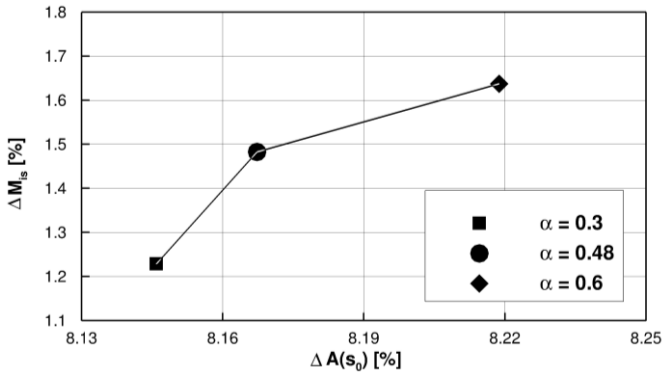

Figure 14: Mach number intensity and throat area variation at OP8

A closer look into Figure 14 shows the same tendency regarding the local shock fluctuations with respect to α. Keeping the eigenfrequency constant while increasing the α-value results in an increased throat area and finally in higher Mach number fluctuations.

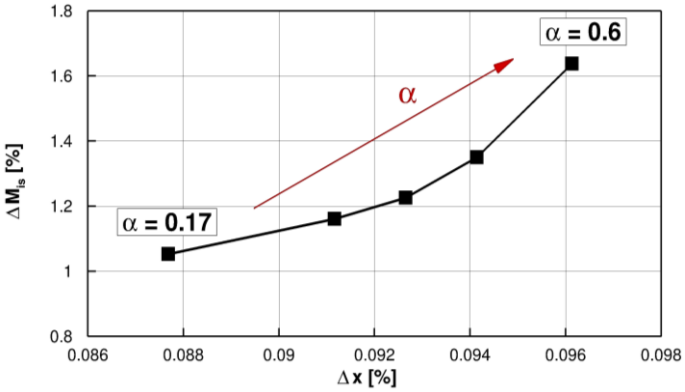

Figure 13: Mach number intensity variation and shock oscillation amplitude at OP8

It must be noted, that transfer of energy from the fluid to the blade occurs if the fluid force is in phase with the velocity of the motion and not the displacement. As it can be seen in Figure 11 for the parameter combination ($f^*= -0.5$ and $\alpha=0.48$), a reduction of α must not necessarily lead to a flutter stability improvement.

CONCLUSIONS

The flutter stability analyses of modified twist/plunge ratios and blade eigenfrequencies were carried out and are based on the energy exchange approach. The linear system behavior assumption was verified by carrying out a blade vibration amplitude analysis. The blade passage number for the ICM model was identified and accurate as well as computationally efficient for the flutter stability predictions. The predicted aerodynamic performance and structural dynamic behavior for the baseline was in a good agreement with the experimental data. The flutter stability method was also validated at 80% part speed. The study show that a mode shape parameter variation strongly affects the flutter stability, which can be summarized as follows:

- A mode shape modification can lead to a shift of the global flutter minimum Λ with respect to the ND.
- An Increased flutter margin was achieved due to blade eigenfrequency variation for $f^* > 0$ at all speed lines with exception for 80% part speed.
- It has been observed that a combination of f^* extrema with a low α ratio ensures a high flutter stability at 80% part speed.
- A reduction of α shows a promising design approach over a wide speed range with a clear tendency.
- However, the role of shocks for the aeroelastic behavior in fans in transonic flow regimes show also a correlation with α and the shock oscillation amplitude.
- Destabilizing effects were observed through the co-action of boundary/layer interactions and separated flows, which were reduced with low twist/plunge ratios.

An assessment and parameter variation over a wide operating range for constant speed lines should be carried out to resolve the whole flutter map and analyze especially the discussed effects also near the choke line. The question rises whether the discussed flutter stability behavior and prediction due to structural modifications will be still valid near the choke line.

NOMENCLATURE

CFD	Computational Fluid Dynamic
FM	Flutter Margin
IBPA	Inter-Blade Phase Angle
BTW	Backward Travelling Wave
FTW	Forward Travelling Wave
Ma	Relative Mach number
ND	Nodal Diameter
DP	Design Point (at Cruise Speed)
TWM	Travelling Wave Mode
UFFA	Universal Fan Facility for Acoustics
1F	First flap mode
EO	Engine Order
BPF	Blade Passing Frequency
N	Shaft speed
$\hat{c}_w$	Influence Coefficient
p	Static Pressure
$\mathbf{n}$	Blade surface normal vector
$\dot{\mathbf{x}}$	Blade velocity

ACKNOWLEDGMENTS

The authors are grateful to AneCom for providing the geometry and performance data of the UFFA-Fan especially Dr. Liesner for providing the unsteady data. The authors would also like to acknowledge the financial support of the industrial partner Rolls-Royce Deutschland and the German Federal Ministry of Economic Affairs and Energy in the frame of the Aeronautical Research Program LuFo (project FanTip, Grant Numbers 20E1304A, 20E1304B, 20E1304C). Numerical simulations were carried out on the High Performance Computing System Cheops at the University of Cologne.

REFERENCES

[1] Vahdati, M., Simpson, G., and Imregun, M., 2011, "Mechanisms for Wide-Chord Fan Blade Flutter," ASME J. Eng. Gas Turbines Power, 133(4)

[2] Stapelfeldt S. and Vahdati M., "On the Importance of Engine-Representative Models for Fan Flutter Predictions.", ASME Paper, 2017

[3] Srinivasan A.V., "Flutter and Resonant Vibration Characteristics of Engine Blades"., ASME. J. Eng. Gas Turbines Power., 1997

[4] Vahdati M., Smith N. and Zhao F., "Influence of Intake on Fan Blade Flutter.", ASME. J. Turbomach., 2015

[5] Zhao F., Nipkau J. and Vahdati M., "Influence of acoustic reflections on flutter stability of an embedded blade row", Part A-Journal of Power an Energy, Vol: 230, Pages: 29-43, 2016

[6] Lee K., Wilson M. and Vahdati M., "Numerical Study on Aeroelastic Instability for a Low-Speed Fan", ASME. J. Turbomach., 2017

[7] Vahdati M. and Cumpsty N., "Aeroelastic Instability in Transonic Fans", ASME. J. Eng. Gas Turbines Power., 2015

[8] Köhler W. The Influence of the TCS on the Circumferential Mode Distribution in the Inlet of a Fanrig (UFFA). ASME. Turbo Expo: Power for Land, Sea, and Air, Volume 8: Turbomachinery, Parts A, B, and C ():1813-1822. doi:10.1115/GT2012-69762.

[9] Mueller, D.; Schulz, H.-J.; Zitouni, G. and Baumann, W.: Europe's Largest Aero Acoustic Test Facility for Aero Engine Fans – The Development and Operation of the AneCom AeroTest Anechoic Chamber. AIAA Paper 2005-3050, 2005

[10] Aulich A.-L., Sauer T., Iseni S., Moreau A., Peitsch D., Mailach R., Micallef D., Enghardt L. and Nicke E., "Fan casing contouring under consideration of aeroacoustics, mechanics, aeroelasticity, and whole engine performance", CEAS aeronautical journal, pp.1-10, 2016

[11] Micallef D., Witteck D., Wiedermann A., Kluß, D. and Mailach R., 2012: "Three-Dimensional Viscous Flutter Analyses of a Turbine Cascade in Subsonic and Transonic Flows", ASME Paper, 2012

[12] Micallef D., Witteck D., Wiedermann A. and Mailach R., "An Efficient Workflow for Accurate Flutter Stability Analyses and Application to a State of the Art Compressor Rotor.", ASME Paper, 2014

[13] Iseni S., Micallef D. and Mailach R., "Investigation of Inlet Distortion on the Flutter Stability of a Highly Loaded Transonic Fan Rotor", ASME Paper, 2016

[14] Witteck D., Micallef D., Wiedermann A., Mailach R., "Three-Dimensional Viscous Flutter Analysis of a Turbine Cascade in Supersonic Flow", ISUAAAT13-S9-2, 13th International Symposium on Unsteady Aerodynamics, Aeroacoustics and Aeroelasticity of Turbomachines, Tokyo, Japan, 2012
[15] Schuff M, Lengyel-Kampmann T, Forsthofer N., "Influence of the Steady Deformation on Numerical Flutter Prediction for Highly Loaded and Flexible Fan Blades. ", ASME Paper, 2017
[16] Srivastava R., Bakhle M. A., and Keith T. G. "Numerical Simulation of Aerodynamic Damping for Flutter Analysis of Turbomachinery Blade Rows", Journal of Propulsion and Power, Vol. 19, No. 2, pp. 260-267, 2003
[17] Srivastava R. and Keith. T. G., "Influence of Shock Wave on Turbomachinery Blade Row Flutter", Journal of Propulsion and Power, Vol. 21, No. 1, pp. 167-174., 2005
[18] Fu Q, Chen ZC. "Medial Axis Transform of Planar Shapes With Free-Form Curve Boundary.", ASME Paper, 2010
[19] Peeren C, Vogeler K. Geometrical Modification of the Unsteady Pressure to Reduce Low-Pressure Turbine Flutter. ASME. *J.* Turbomach.2017;139(9)

APPENDIX A – Grid details

Table A1: Details of the computational grids

Blade Passage	Grid A	Grid B	Grid C
Grid points along blade	107	129	155
Grid points at LE and TE	7	9	11
Spanwise Grid points (tip)	61 (11)	81 (14)	111 (17)
y^+on blade walls	20	10	7.5
Min. cell angle [°]	30	27	28
Max. volume change	6	3.8	3.4
Tot. number of nodes	$430 \cdot 10^3$	$530 \cdot 10^3$	$640 \cdot 10^3$
Total pressure ratio	1.526	1.531	1.532

APPENDIX B – Channel area kinematic and displacement components

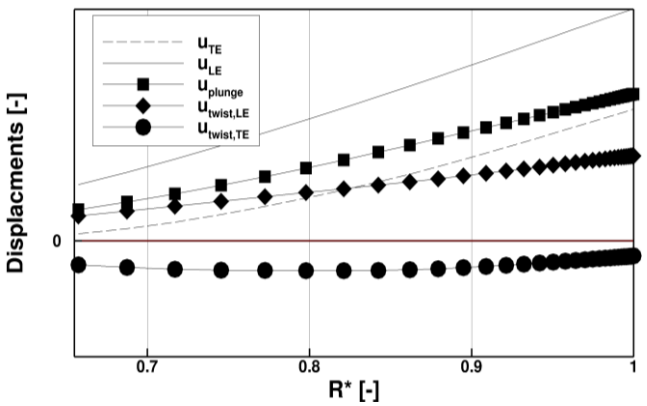

Figure B1: Modal displacements vs. blade span at OP8

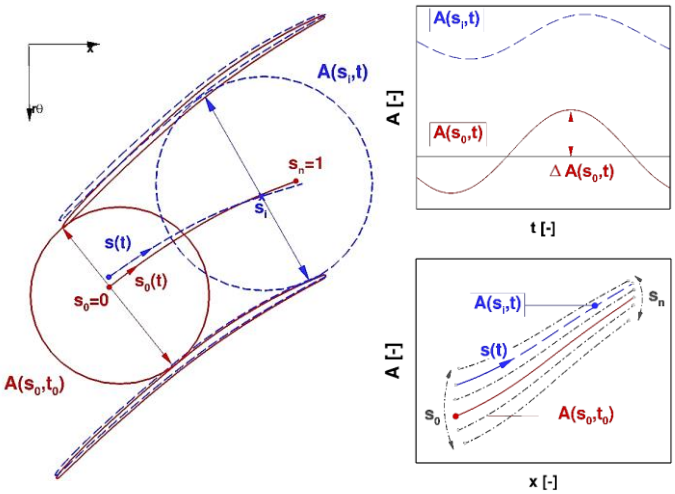

Figure B2: Channel area kinematic during blade oscillation